THE JOURNAL OF PHYSICAL CHEMISTRY B
A JOURNAL OF THE AMERICAN CHEMICAL SOCIETY

pubs.acs.org/JPCB
Article

Emission Intensity Enhancement for Iridium(III) Complex in Dimethyl Sulfoxide under Photoirradiation

Shingo Hattori, Shuntaro Hirata, and Kazuteru Shinozaki*

Cite This: https://doi.org/10.1021/acs.jpcb.1c03753

ABSTRACT: We found emission intensity enhancement for *fac*-Ir(ppy)$_3$ (ppy = 2-(2′-phenyl)pyridine) in aerated dimethyl sulfoxide (DMSO) during photoirradiation for the first time. This phenomenon was concluded to be responsible for the consumption of $^3O_2$ dissolved in DMSO through dimethyl sulfone production by photosensitized reaction using *fac*-Ir(ppy)$_3$. A $^3O_2$ adduct of DMSO molecule was detected by UV absorption measurement and theoretical calculation. We proposed a mechanism for the emission enhancement reaction including $^{1,3}O_2$ molecules and $^{1,3}O_2$-DMSO adducts and validated it through a simulation of emission intensity change using an ordinary differential equation solver.

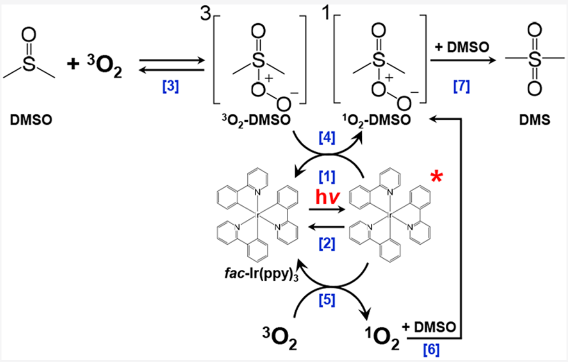

■ INTRODUCTION

Transition metal complexes attract great attention not only to inorganic chemists but also material, medicinal, and organic chemists because of the strong emission suitable for organic light emitting diode (OLED),[1−7] the photodynamic therapy (PDT) using singlet oxygen,[8,9] and the discovery of new synthetic method using their photocatalytic ability,[10−22] respectively. In particular, phosphorescent metal complexes have been actively developed for application utilizing their characteristics of the long-lived strong photoemission. *fac*-Ir(ppy)$_3$ (ppy = 2-(2-phenyl)pyridine), one of the typical examples of them, has been vigorously investigated since the demonstration of OLED green emitter by Baldo et al. in 1990.[4] The long-lived triplet excited state of *fac*-Ir(ppy)$_3$ is also expected to be employed to the emission probe,[23,24] the photosensitization for photodynamic therapy and photocatalysis of the photochemical reactions.

The excited *fac*-Ir(ppy)$_3$ effectively transfers its energy to ground oxygen molecule ($^3O_2$) via the Dexter's mechanism, where the overlapping of electronic clouds between *fac*-Ir(ppy)$_3$* and $^3O_2$ induces the production of singlet oxygen molecule ($^1\Delta_g$) by the direct electron exchange. In 2019, Soni et al. reported a new synthesis method to afford spiro-azalactams analogues using the photosensitized $^1O_2$ by *fac*-Ir(ppy)$_3$ in dimethyl sulfoxide (DMSO).[20] Also, the same photosensitization system of *fac*-Ir(ppy)$_3$ and $^1O_2$ in DMSO has been applied to PDT inducing a cell death.[21] Although the versatility of *fac*-Ir(ppy)$_3$ in a photochemical reaction has been demonstrated, the reaction mechanism has not been investigated in detail so far. DMSO has been widely used as a solvent of organic syntheses and PDTs because of a low toxicity, a high polarity, and a capability of dissolving many compounds,[20−22] whereas there is no report on the role of DMSO in the photosensitization process.

Here, we report an emission intensity enhancement of *fac*-Ir(ppy)$_3$ in DMSO solution containing O_2 under photoirradiation for the first time. The enhancement is not confirmed in deoxygenated DMSO solution of *fac*-Ir(ppy)$_3$ and other organic solvents. Moreover, when employing a DMSO solution containing $[Ru(bpy)_3]^{2+}$ (bpy = 2,2′-bipyridine) instead of *fac*-Ir(ppy)$_3$, the emission enhancement is observed as well. These results suggest that a photoreaction of DMSO molecule with dissolved oxygen takes place by the aid of excited *fac*-Ir(ppy)$_3$ as a photosensitizer. ^1H NMR indicates that the product of a photochemical reaction is dimethyl sulfone (DMS). $^3O_2$-DMSO adduct is a key intermediate of the photoproduction of DMS, supported by experimental electronic absorption spectrum and theoretical calculations using time-dependent density functional theory (TD-DFT). A proposed mechanism may provide new insight for understanding photocatalytic organic syntheses using *fac*-Ir(ppy)$_3$ in DMSO (Scheme 1).

Received: April 26, 2021
Revised: July 25, 2021

Scheme 1. Reaction Scheme for Production of DMS from DMSO and $^3O_2$ by the Photosensitization of *fac*-Ir(ppy)$_3$

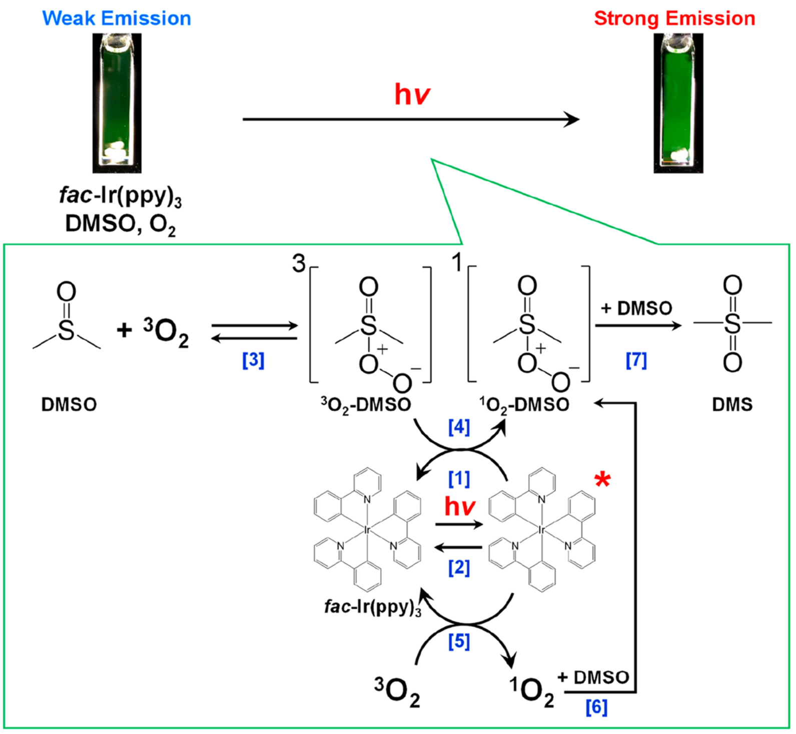

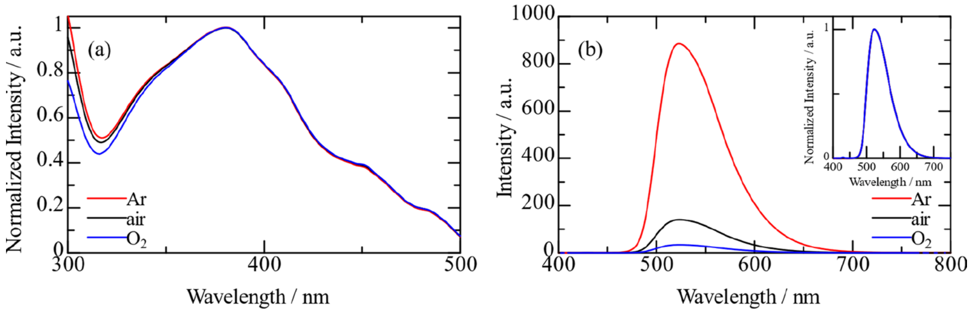

Figure 1. (a) Excitation and (b) emission spectra of *fac*-Ir(ppy)$_3$ (2.20×10^{-5} M) in Ar (red), air (black), and O_2 (blue) saturated DMSO at room temperature. Inset is the emission spectra normalized at peaks, which are identical to each other.

■ METHODS

Materials. *fac*-Ir(ppy)$_3$ was synthesized as reported in a previous method.[6] A mixture of $IrCl_3 \cdot nH_2O$ (101 mg, 0.34 mmol) and 2-phenylpyridine (108 mg, 0.70 mmol) in a mixed solvent of water (1.5 mL) and 2-ethoxyethanol (4.5 mL) was stirred at 105 °C under Ar atmosphere for 15 h. After cooling to room temperature, the resulting precipitate was filtered off and washed with methanol. The yield of $[Ir(ppy)_2Cl]_2$ was 65% (123 mg, 0.11 mmol). ^1H NMR (400 MHz, CD_2Cl_2) for $[Ir(ppy)_2Cl]_2$: δ 9.25 (d, 1H, J = 4.8 Hz), δ 7.94 (d, 1H, J = 8.0 Hz), δ 7.80 (t, 1H, J = 7.8 Hz), δ 7.56 (d, 1H, J = 8.0 Hz), δ 6.85−6.79 (m, 2H), δ 6.60 (t, 1H, J = 7.4 Hz), δ 5.87 (d, 1H, J = 8.0 Hz). Following the previous methods, $[Ir(ppy)_2Cl]_2$ (85 mg, 0.08 mmol), 2-phenylpyridine (59 mg, 0.38 mmol), acetylacetone (17 mg, 0.17 mmol), and triethylamine (21 mg, 0.21 mmol) were added to ethylene glycol (5 mL) and the solution was degassed by Ar bubbling prior to heat at 175 °C with stirring for 20 h. After cooling to room temperature, the precipitate was filtered off, washed with water and ethanol, and then purified by passing through a silica gel column followed by elution with chloroform. The resulting yellow solution was dried using a rotary evaporator, and the solid was recrystallized from dichloromethane/hexane. The yield of *fac*-Ir(ppy)$_3$ was 45% (47 mg, 0.07 mmol). ^1H NMR (400 MHz, CD_3CN) δ 8.01 (d, 1H, J = 8.4 Hz), δ 7.75−7.71 (m, 2H), δ 7.60 (d, 1H, J = 5.2 Hz), δ 7.00 (t, 1H, J = 6.4 Hz), δ 6.86 (t, 1H, J = 7.4 Hz), δ 6.75 (t, 1H, J = 7.0 Hz), δ 6.69 (d, 1H, J = 8.4 Hz).

Instrumental Techniques. ^1H NMR spectra were measured using a Bruker AVANCE III HD (400 MHz) and analyzed by a TopSpin 3.5 pl7 software. UV−vis spectra were measured using a JASCO spectrophotometer V-530ST. Emission and excitation spectra were recorded on a JASCO spectrofluorometer FP-6500ST equipped by a Peltier thermo-controller. Sample solutions in a quartz cell attached with a greaseless valve were aerated, degassed, or oxygenated by the appropriate gas bubbling for 20 min prior to the UV and emission measurements. Emission lifetimes were determined through single-exponential curve-fitting of emission intensity data recorded over time with a Tektronics TBS 1052B-EDU digital oscilloscope after pulsed excitation at 355 nm using a Continuum Surelite Nd:YAG laser. Detection of emission intensity during photoirradiation was carried out using a

JASCO spectrofluorometer FP-6500ST. During photoirradiation with monochromatic 380 nm light from 150 W xenon lamp, emission intensity change was measured while stirring the gas-saturated solution and the temperature was adjusted using a Peltier thermocontroller. White light of a USIO Xe short-arc lamp (150 W) through water as a thermal-cut filter was employed to prepare a photoproduct. The obtained photoproduct was monitored with a Bruker NMR AVANCE III HD (400 MHz).

Computational Details. The geometry optimization was carried out by density functional theory (DFT) calculation. The B3LYP as a functional and the basis set of 6-31G* for H, C, N, O, S and LANL2DZ for Ir were employed in the calculation. Polarizable continuum model (PCM) was taken into account for the solvent effect by DMSO on total energy. The absorption spectra were simulated by time-dependent density functional theory (TD-DFT) calculation using the optimized structures. Here the B3LYP as a functional and the basis set of 6-31G* for H, C, N, O, and S were employed in the calculation. All calculations were carried out by Gaussian 16 package. The fitting simulation of differential equations was carried out using MATLAB.

■ RESULTS AND DISCUSSION

Emission Intensity Enhancement for *fac*-Ir(ppy)$_3$. Figure 1a,b shows excitation and emission spectra of 2.02 × 10^{-5} M *fac*-Ir(ppy)$_3$ in air, Ar, and O_2 saturated DMSO solutions at 293 K. The excitation peaks attributed to a transition from metal to ligand charge transfer (MLCT) were observed at 380 nm (Figure 1a), and the emission peaks assigned to MLCT phosphorescence were observed at 523 nm (Figure 1b).[2,5] For emission spectra, the spectral profiles are consistent with each other showing an emission peak at 523 nm although the emission intensities are observed to be in the order of O_2 < air < Ar saturated DMSO. Emission lifetimes evaluated from curve fitting of emission decay curves as τ = 1.38 μs (Ar), 182 ns (air), 35.4 ns (O_2). The variation in emission lifetime is mainly responsible for the emission quenching by dissolved $^3O_2$. Assuming the quenching is a diffusion-controlled process where quenching rate constant (k_q) is typically $k_q = 1 \times 10^9$ to 1×10^{10} M^{-1} s^{-1},[25,26] the concentration of the quencher is roughly estimated as 3×10^{-3} to 3×10^{-2} M from the Stern−Volmer relation (see Supporting Information for details on Stern−Volmer relation). On the other hand, self-quenching of emission is well-known for *fac*-Ir(ppy)$_3$ because of the long-lived triplet excited state. Emission decays of *fac*-Ir(ppy)$_3$ in DMSO were measured while changing the concentration from 1.01×10^{-5} M to 6.05×10^{-5} M. In polar solvent, the self-quenching of emission is caused by the ground *fac*-Ir(ppy)$_3$ but not triplet−triplet annihilation.[27−31] Evaluated emission lifetime from curve fittings using single exponential functions are listed in Table 1. From a Stern−Volmer plot for the self-quenching (Figure S1), the self-quenching rate and the lifetime at infinite dilution are determined as $k_{sq} = 1.25 \times 10^9$ M^{-1} s^{-1} and τ_0 = 1.45 μs (see Supporting Information for details on Stern−Volmer plot).

Table 1. Concentration Dependence in Emission Lifetime of *fac*-Ir(ppy)$_3$ in Ar Saturated DMSO

[*fac*-Ir(ppy)$_3$]/M	6.05×10^{-5}	4.03×10^{-5}	2.02×10^{-5}	1.01×10^{-5}
τ/μs	1.31	1.35	1.41	1.42

Figure 2 shows time-profiles of emission intensity of *fac*-Ir(ppy)$_3$ at 523 nm under photoirradiation of O_2 saturated DMSO, acetonitrile, ethyl acetate, and toluene solution (2.02×10^{-5} M) at 293 K for 10 800 s using UV light (λ_{ex} = 380 nm). Surprisingly, the emission intensity of *fac*-Ir(ppy)$_3$ was enhanced under photoirradiation in O_2 saturated DMSO solution while that did not change in other solvents such as acetonitrile, ethyl acetate, and toluene. The remarkable emission intensity change observed after photoirradiation to *fac*-Ir(ppy)$_3$ in O_2 saturated DMSO solution showed an almost linear line as a function of *t*. From the slope of the straight line, the rate in emission enhancement was determined to be 1.06×10^{-3} s^{-1}. For other solvents, the rates evaluated from the respective slopes were negligibly small, 3.08×10^{-6} s^{-1} (acetonitrile), 3.14×10^{-6} s^{-1} (ethyl acetate), and -5.10×10^{-6} s^{-1} (toluene), which are 1000 times smaller than that for DMSO solution. Since the entire solutions were O_2 gas saturated, emission from photoexcited *fac*-Ir(ppy)$_3$ (*fac*-Ir(ppy)$_3$*) should be strongly quenched by the triplet−triplet energy transfer, which are frequently observed for phosphorescent materials. This emission enhancement suggests that the photoirradiation to *fac*-Ir(ppy)$_3$ in DMSO solution can suppresses the emission quenching by $^3O_2$. The emission intensity enhancement was observed even in a DMSO solution containing $[Ru(bpy)_3]^{2+}$ (bpy = 2,2′-bipyridine) instead of *fac*-Ir(ppy)$_3$ (Figure S2).

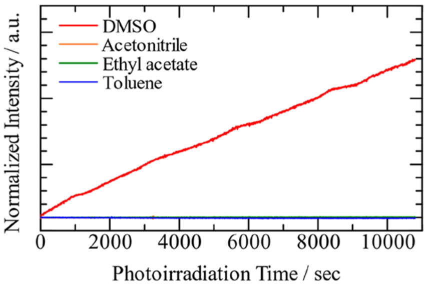

Figure 2. Time-profiles of emission intensity at 523 nm of *fac*-Ir(ppy)$_3$ in O_2 saturated DMSO (red), acetonitrile (orange), ethyl acetate (green), toluene solution (blue) under photoirradiation (2.02×10^{-5} M, 293 K, λ_{ex} = 380 nm). Here, the intensities at *t* = 0 s are normalized to unity.

Emission enhancement was observed with changing excitation wavelength by every 20 nm from 280 to 480 nm for an O_2 saturated DMSO solution containing *fac*-Ir(ppy)$_3$ (Figure 3a). Figure 3b shows action spectra of the photoreaction at 0, 2000, 4000, 6000, 8000, and 10000 s, which are plots of emission intensity against the irradiation light wavelength. The action spectrum at *t* = 0 corresponds to the excitation spectrum of *fac*-Ir(ppy)$_3$, consistent with absorption spectrum of *fac*-Ir(ppy)$_3$ (Figure 6). These plots clearly show that the emission intensity increases along with irradiation time. Here, the emission intensity was increased by irradiation at emission peak, indicating that *fac*-Ir(ppy)$_3$* as a photosensitizer plays a key role of the emission enhancement and the enhancement is accelerated with increasing the number of *fac*-Ir(ppy)$_3$*. Figure 4 shows plots of emission intensities against irradiation time when the concentration of *fac*-Ir(ppy)$_3$ was varied from 4.00×10^{-6} to 1.00×10^{-4} M in O_2 saturated DMSO. Emission intensity was increased by increasing the

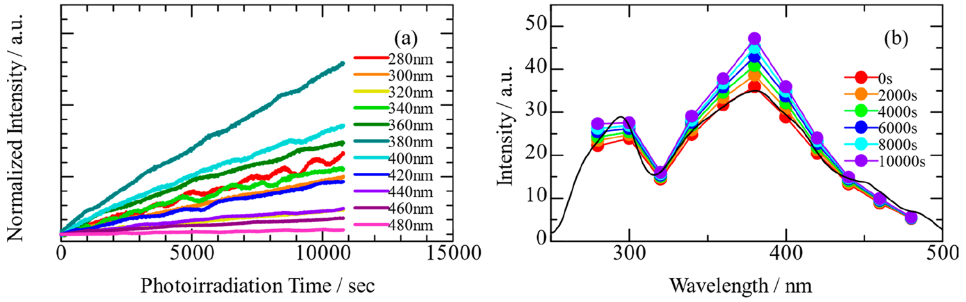

Figure 3. (a) Time-profiles of emission intensity at 523 nm of *fac*-Ir(ppy)$_3$ at a variety of excitation wavelengths in O_2 saturated DMSO, and (b) action spectra for emission intensity enhancement of *fac*-Ir(ppy)$_3$ (2.02×10^{-5} M) in O_2 saturated DMSO upon photoirradiation with the excitation spectrum (black line). In (a), the intensities at $t = 0$ s are normalized to unity.

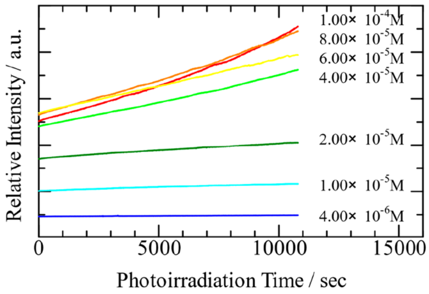

Figure 4. Time-profiles of emission intensity at 523 nm of *fac*-Ir(ppy)$_3$ at a variety of concentrations in O_2 saturated DMSO (293 K, λ_{ex} = 380 nm).

concentration, which is consistent with the results of excitation wavelength dependence in emission enhancement.

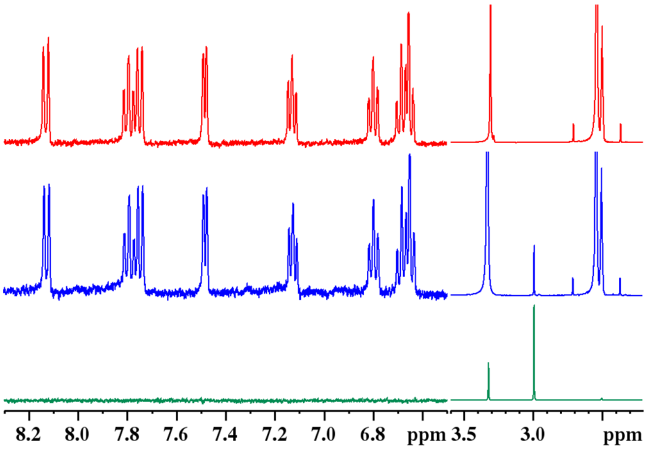

Figure 5. ^{1}H NMR of *fac*-Ir(ppy)$_3$ in 500 μL of DMSO-d_6 containing 5 μL of DMSO-h_6 before (red) and after photoirradiation (blue), and ^{1}H NMR of DMS in DMSO-d_6 (green).

^{1}H NMR measurement was measured for *fac*-Ir(ppy)$_3$ in a mixture of DMSO-d_6 and DMSO-h_6 (v/v = 100/1) before and after photoirradiation as shown in Figure 5. The spectrum in the region of aromatic proton for *fac*-Ir(ppy)$_3$ after photoirradiation was very similar to that before photoirradiation. On the other hand, a new singlet peak was observed at 2.99 ppm. This peak can be assigned to protons of dimethyl sulfone (DMS), because it is in good agreement with that of commercial DMS in DMSO-d_6 (Figure 5, green). On the other hand, the peak at 2.99 ppm was not observed after photoirradiation of O_2-saturated DMSO-d_6/DMSO-h_6 (v/v = 100/1) solution without *fac*-Ir(ppy)$_3$ (Figures S3 and S4). These results clearly show that the photoirradiation of *fac*-Ir(ppy)$_3$ in O_2 saturated DMSO provides DMS without changing the structure of *fac*-Ir(ppy)$_3$ (Scheme 1). The emission intensity of *fac*-Ir(ppy)$_3$ increases by the consumption of O_2 in this reaction.

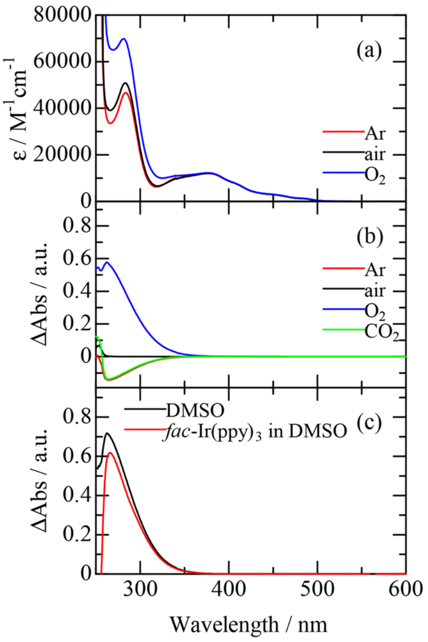

Figure 6. (a) UV−vis absorption spectra of *fac*-Ir(ppy)$_3$ in Ar, air, O_2 saturated DMSO. (b) UV absorption spectra of Ar, air, O_2 and CO_2 gas saturated DMSO. The spectrum of air saturated DMSO was employed as a baseline. (c) A difference spectrum (black) between O_2 saturated and Ar saturated DMSO and that (red) containing *fac*-Ir(ppy)$_3$.

Detection of $^3O_2$ Adduct. Figure 6a shows UV−vis absorption spectra of *fac*-Ir(ppy)$_3$ (2.20×10^{-5} M) in air, Ar, and O_2 saturated DMSOs measured at room temperature (method for details on preparation of variable saturated oxygen concentration in DMSO). The $\pi-\pi^*$ absorption bands at around 280 nm and MLCT bands at around 380 nm were observed for the entire solutions.[18] Although these absorption spectra resemble each other, absorption coefficients in the shorter wavelength region (λ < 380 nm) are in the order Ar < air < O_2 saturated solutions. For air- and O_2-saturated solutions, a distinctive shoulder at 260 nm was observed (Figure 6c, Figure S5). Peak wavelengths (λ_{abs}) and absorption coefficients (ε) at peaks for the absorption spectra are listed in Table 2. When the once O_2-saturated solution was purged with Ar gas to remove dissolved O_2, the $\pi-\pi^*$ absorption band was decreased in intensity to be consistent with that of the Ar saturated solution. This trend in ε at around 280 nm is associated with the concentration of dissolved O_2 in DMSO. However, O_2 molecule does not absorb light in the region of 240−380 nm light but <240 nm. Since absorption spectra ($\lambda >$ 380 nm) for the entire gas-saturated solutions are consistent with each other, it is suggested that the change in absorption spectra is not attributed to the O_2 adduct formation of *fac*-Ir(ppy)$_3$ but some reaction of O_2 with DMSO as a solvent.

Table 2. Absorption Coefficients (ε) at Peak in UV-vis Spectra of *fac*-Ir(ppy)$_3$ in Ar, air, O_2 Saturated DMSO

	ε/M^{-1} cm^{-1} (λ_{abs}/nm)	ε/M^{-1} cm^{-1} (λ_{abs}/nm)
Ar	4.98×10^4 (284)	1.41×10^4 (377)
air	5.50×10^4 (283)	1.41×10^4 (377)
O_2	7.14×10^4 (281)	1.42×10^4 (376)

UV absorption spectra for air, Ar, O_2, and CO_2 saturated DMSO at room temperature using the spectrum of air saturated DMSO as a baseline are shown in Figure 6b. For Ar and CO_2 saturated DMSO, the spectral profiles are coincident with each other, and absorption coefficients below 350 nm are negative and peak wavelengths are both 264 nm. On the contrary, for the O_2 saturated DMSO the absorbance is positive even below 350 nm and shows a peak at 262 nm. These results strongly suggest that the absorption band at around 260 nm rose from the adduct formation of O_2 and DMSO, which takes place even in the air saturated DMSO. Since the absorption intensity at 260 nm is easily modulated by the O_2 concentration, O_2 and DMSO would be loosely attached with each other to produce an adduct via the chalcogen-chalcogen interaction (O_2-DMSO),[32−34] and the O_2-adduct and O_2 would be in an equilibrium state. Figure 6c shows a difference spectrum by subtraction of the spectrum of O_2 saturated DMSO from that of Ar saturated one, and another difference spectrum prepared by the subtraction of the spectrum of O_2 saturated DMSO containing *fac*-Ir(ppy)$_3$ from that of Ar saturated one. These difference spectra are very similar to each other, suggesting that the O_2-DMSO adduct is stable even in the coexistence of *fac*-Ir(ppy)$_3$ and the interaction between *fac*-Ir(ppy)$_3$ and the adduct is negligibly weak. Assuming the ε = 100−1000 at 260 nm, the concentration of $^3O_2$-DMSO adduct is estimated to be 6×10^{-5} -6×10^{-4} M.

To clarify the origin of the absorption band observed at around 260 nm in O_2-DMSO, the simulation of absorption spectrum of O_2-DMSO using time-dependent density functional theory (TD-DFT) calculation was carried out. Here, the optimized geometry of O_2-DMSO was employed for TD-DFT calculation. Figure 7 shows calculated UV absorption spectra of $^3O_2$-DMSO, DMSO, and $^3O_2$ in DMSO. An absorption band at 265.2 nm appeared for $^3O_2$-DMSO alone, while the other bands at 258.5, 239.2, and 226.5 nm of $^3O_2$-DMSO are very similar to those of ^{1}DMSO. Any absorption bands of $^3O_2$ does not appear in the region of 200−300 nm. The lowest absorption at 265.2 nm of $^3O_2$-DMSO is in good agreement with the experimentally observed band at 265 nm for the O_2 saturated DMSO. The electronic transition at 265.2 mn was assinged to be mainly HOMO−2 → LUMO with $f = 8.0 \times 10^{-4}$, where HOMO-2 is a localized orbital on DMSO moiety and LUMO is localized on O_2 as shown in Figure S6. These cacluations support the formation of O_2-DMSO in O_2-saturated DMSO solution.

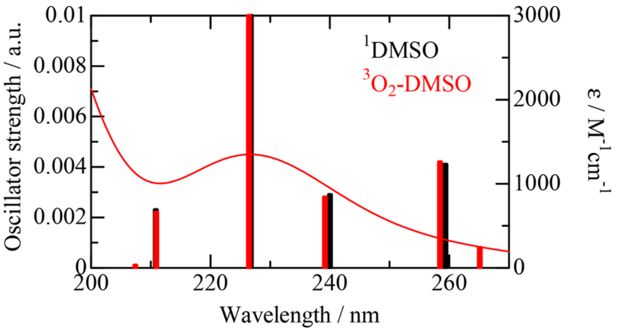

Figure 7. Calculated absorption line spectra of ^{1}DMSO (black) and $^3O_2$-DMSO (red) in DMSO. No absorption band of $^3O_2$ was predicted to appear in the region of 200−300 nm. Red solid line is a calculated absorption spectrum of $^3O_2$-DMSO obtained by multiplying the line spectrum by a Gaussian function.

Reaction Mechanism. To clarify the detailed reaction mechanism, a quantum chemical calculation based on the density functional theory (DFT) was carried out. The energy of O_2, DMSO, O_2-DMSO, and DMS in optimized structures is shown in Figure 8. Here, the energy predicted by the calculation is relatively described using the sum of these energies as an offset ($E(^3O_2, {}^1\mathrm{DMSO}) = 0$ kcal/mol). The energy of singlet O_2-DMSO ($^1O_2$-DMSO) was 34.0 kcal/mol higher than the sum of the energy of singlet DMSO (^{1}DMSO) and triplet O_2 ($^3O_2$). On the other hand, the energy of triplet O_2-DMSO ($^3O_2$-DMSO) was 0.41 kcal/mol lower than the sum of the energy of ^{1}DMSO and $^3O_2$ (the equilibrium constant is estimated as $K = 1.04$ M^{-1}). This indicates that $^3O_2$-DMSO is formed spontaneously from ^{1}DMSO and $^3O_2$. This is consistent with the result that the observed UV absorption in O_2 saturated DMSO solution is due to the formation of O_2-DMSO. The singlet−triplet energy difference in O_2-DMSO was 34.4 kcal/mol. The lower energy difference compared with the excitation energy of *fac*-Ir(ppy)$_3$ (53.7 kcal/mol) implies that the possibility of energy transfer from *fac*-Ir(ppy)$_3$*. The energy of singlet DMS was 23.3 kcal/mol lower than that of $^1O_2$-DMSO. Therefore, the reaction route (Figure 8, red) involving with $^3O_2$-DMSO is proposed as follows: (1) $^3O_2$-DMSO is spontaneously formed from ^{1}DMSO and $^3O_2$, (2) $^1O_2$-DMSO is generated by the energy transfer from *fac*-Ir(ppy)$_3$*, and (3) DMS is spontaneously produced from $^1O_2$-DMSO. On the other hand, the reaction involving with $^1O_2$ is possible because *fac*-Ir(ppy)$_3$ can generate $^1O_2$,[20,21] and the energy of $^1O_2$-DMSO is 5.0 kcal/mol lower than the sum of the energy of ^{1}DMSO and $^1O_2$. This reaction route is illustrated as a blue broken line in Figure 8. (4) $^1O_2$ is generated by the energy transfer from *fac*-Ir(ppy)$_3$*, (5) $^1O_2$-DMSO is spontaneously formed from ^{1}DMSO and $^1O_2$.

To confirm the validity of the proposed reaction mechanism, curve fitting of time-profiles of emission intensity at 523 nm of *fac*-Ir(ppy)$_3$ in O_2 saturated DMSO using deferential equations based on the proposed reaction mechanism (Scheme 1) was carried out (Supporting Information for details on the deferential equations). Figure 9a,b shows the emission intensity enhancement curves as open circles depending on the excitation wavelength and the concentration of *fac*-

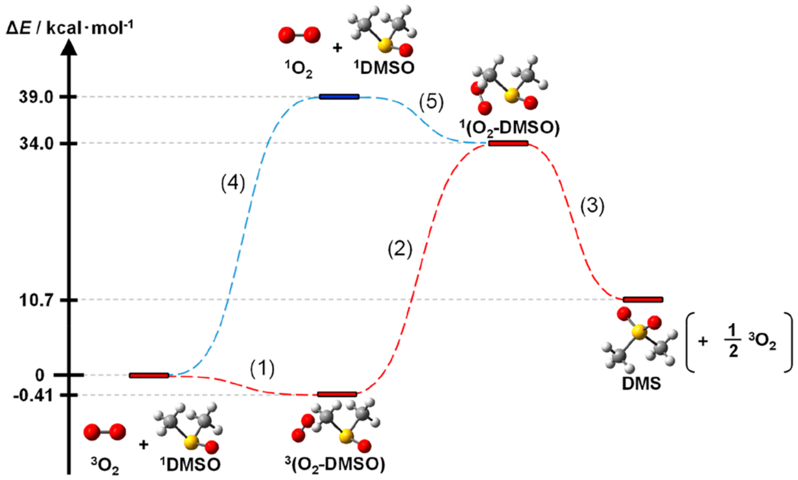

Figure 8. Schematic energy diagram for the photosensitization reaction affording DMS from DMSO and $^3O_2$. Here, the energy predicted by the calculation is relatively described using the sum of these energies as an offset ($E(^3O_2$, ^{1}DMSO) = 0 kcal/mol).

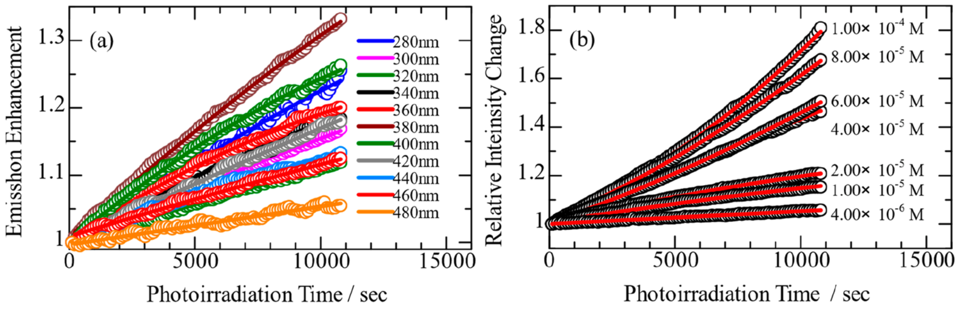

Figure 9. (a) Excitation dependence in emission enhancement for *fac*-Ir(ppy)$_3$ (2.02 × 10^{-5} M) in O_2 saturated DMSO as open circles. Intensities are normalized at t = 0. Simulation results are plotted as solid lines, which are changes in [Ir(ppy)$_3$*] as a function of t. (b) Concentration dependence in emission enhancement for *fac*-Ir(ppy)$_3$ in O_2 saturated DMSO as open circles. Intensities are normalized at t = 0. Simulation results are plotted as solid lines, which are changes in [Ir(ppy)$_3$*] as a function of t.

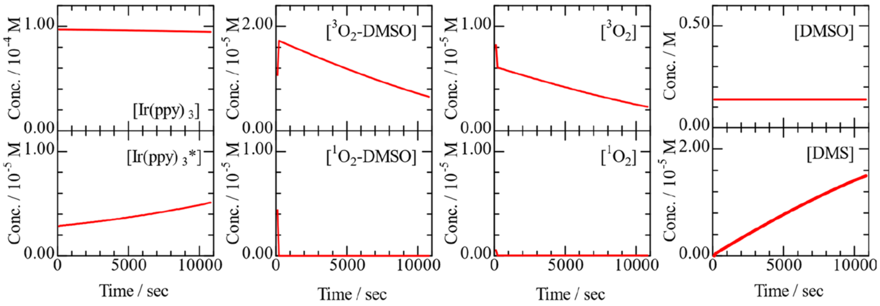

Figure 10. Simulation for the emission enhancement for *fac*-Ir(ppy)$_3$ (1.00 × 10^{-4} M) in O_2 saturated DMSO. Simulation results are displayed in red lines against t, which are changes in concentration of species contributing to the photoreaction. The variations in concentration are obtained using the rate constants of $k_0 = 2.40 \times 10^7$ s^{-1}, $k_1 = 1.00 \times 10^6$ s^{-1}, $k_2 = 6.69 \times 10^8$ M^{-1} s^{-1}, $k_3 = 2.45 \times 10^{10}$ M^{-1} s^{-1}, $k_4 = 1.51 \times 10^8$ M^{-1} s^{-1}, $k_{-4} = 2.55 \times 10^{10}$ s^{-1}, $k_5 = 4.96 \times 10^{10}$ M^{-1} s^{-1}, $k_6 = 7.00 \times 10^6$ s^{-1}, $k_7 = 9.00 \times 10^8$ M^{-1} s^{-1}, $k_8 = 1.88 \times 10^{10}$ M^{-1} s^{-1}, $k_9 = 3.00 \times 10^6$ M^{-1} s^{-1}, where these rate constants are converted so that k_1 matches the reciprocal of emission lifetime (t = 1 μs) of *fac*-Ir(ppy)$_3$.

Ir(ppy)$_3$, respectively, and their simulation results displayed as solid lines. For both, the simulation and experimental result are in very good agreement with each other. These results strongly suggest the validity of proposed mechanism for the emission intensity enhancement.

Figure 10 shows simulation results for emission intensity enhancement in photoirradiation of 1.00 × 10^{-4} M *fac*-Ir(ppy)$_3$, where simulated values have been converted to concentrations so as to be [Ir(ppy)$_3$*] + [Ir(ppy)$_3$] = 1.00 × 10^{-4} M. [Ir(ppy)$_3$*] increases its own concentration while proceeding with the reaction, corresponding to the emission intensity enhancement. This emission intensity enhancement is reasonably accounted by the suppress of emission quenching due to the decrease in concentrations of $^3O_2$ and $^3O_2$-DMSO capable of quenching of emission from *fac*-Ir(ppy)$_3$*. [$^3O_2$-DMSO] is always three time larger than [$^3O_2$] during the reaction, which indicates an equilibrium between them. The concentrations of $^3O_2$ and $^3O_2$-DMSO suddenly decrease and increase, respectively, at very early stage of simulated reaction. These sudden changes in concentration are considered to correspond to the fast process toward the achievement of equilibrium of the adduct formation of $^3O_2$ with DMSO molecule. For $^1O_2$ and $^1O_2$-DMSO species, being expectedly very reactive, their concentrations are predicted to be almost zero during the whole reaction process. This result suggests that the $^1O_2$ and $^1O_2$-DMSO are the transient species and the steady-state approximation can be applied to the $d[^1O_2]/dt$ and $d[^1O_2\text{-DMSO}]/dt$ in the differential equations. [DMSO] is considerably larger than those of other species and almost constant during the reaction, which is agreement with the fact that DMSO is solvent. The photoproduct DMS is gradually increased in concentration with proceeding the reaction. Therefore, we can summarize the emission enhancement reaction during the photoirradiation of *fac*-Ir(ppy)$_3$ in O_2 saturated DMSO as Scheme 1.

CONCLUSIONS

In this study, we found the emission intensity enhancement for *fac*-Ir(ppy)$_3$ in DMSO containing molecular oxygen. This phenomenon was reasonably accounted by the $^3O_2$ consumption through dimethyl sulfone formation in the photosensitized reaction due to *fac*-Ir(ppy)$_3$*. To the best of our knowledge, we detected for the first time $^3O_2$-DMSO adduct, easily prepared at ambient condition when $^3O_2$ is dissolved in DMSO. Photoirradiation to $^3O_2$ and triplet sensitizer in DMSO system potentially has the capability of activating $^3O_2$-DMSO to labile $^1O_2$-DMSO to oxidize some substrates as well as $^1O_2$. We proposed the reaction mechanism for the emission intensity enhancement including transient species $^1O_2$ and $^1O_2$-DMSO adduct. The simulation predicting concentration of Ir(ppy)$_3$* in the photoreaction well reproduced the emission intensity change even when the concentration of *fac*-Ir(ppy)$_3$ and the excitation wavelength were varied. As well, the simulation provided the concentration change in other species including the labile transients $^1O_2$ and $^1O_2$-DMSO of which concentrations are almost zero during the photoreaction. It might be careful that $^1O_2$-DMSO adduct could participate in the oxidation of substrate in the organic syntheses and/or in the cell death in PDTs using the system of O_2, triplet sensitizer, and DMSO.

ASSOCIATED CONTENT

Supporting Information

The Supporting Information is available free of charge at https://pubs.acs.org/doi/10.1021/acs.jpcb.1c03753.

> Stern−Volmer plot, emission spectra of [Ru(II)(bpy)$_3$]-Cl$_2$, ^{1}H NMR of DMSO, UV−vis spectrum of fac-Ir(ppy)$_3$, DFT calculations, simulation details (PDF)

AUTHOR INFORMATION

Corresponding Author

Kazuteru Shinozaki − *Graduate School of Nanobioscience, Yokohama City University, Kanazawa-ku, Yokohama 236-0027, Japan;* orcid.org/0000-0001-7571-9210;
Email: shino@yokohama-cu.ac.jp

Authors

Shingo Hattori − *Graduate School of Nanobioscience, Yokohama City University, Kanazawa-ku, Yokohama 236-0027, Japan;* orcid.org/0000-0002-9385-961X

Shuntaro Hirata − *Graduate School of Nanobioscience, Yokohama City University, Kanazawa-ku, Yokohama 236-0027, Japan*

Complete contact information is available at:
https://pubs.acs.org/10.1021/acs.jpcb.1c03753

Notes

The authors declare no competing financial interest.

ACKNOWLEDGMENTS

This work was supported by JSPS KAKENHI (Grants JP17H06375 and JP21K14647).

REFERENCES

(1) Sprouse, S.; King, K. A.; Spellane, P. J.; Watts, R. J. Photophysical Effects of Metal-Carbon Sigma Bonds in Ortho-metalated Complexes of Iridium(III) and Rhodium(III). *J. Am. Chem. Soc.* **1984**, *106*, 6647−6653.

(2) King, K. A.; Spellane, P. J.; Watts, R. J. Excited-state Properties of a Triply Ortho-metalated Iridium(III) Complex. *J. Am. Chem. Soc.* **1985**, *107*, 1431−1432.

(3) King, K. A.; Watts, R. J. Dual Emission from an Ortho-metalated Iridium(III) Complex. *J. Am. Chem. Soc.* **1987**, *109*, 1589−1590.

(4) Baldo, M. A.; Thompson, M. E.; Forrest, S. R. High-efficiency Fluorescent Organic Light-emitting Devices Using a Phosphorescent Sensitizer. *Nature* **2000**, *403*, 750−753.

(5) Hofbeck, T.; Yersin, H. The Triplet State of fac-Ir(ppy)$_3$. *Inorg. Chem.* **2010**, *49*, 9290−9299.

(6) Takayasu, S.; Suzuki, T.; Shinozaki, K. Intermolecular Interactions and Aggregation of fac-Tris(2-phenylpyridinato-C^2,*N*)-iridium(III) in Nonpolar Solvents. *J. Phys. Chem. B* **2013**, *117*, 9449−9456.

(7) Ito, W.; Hattori, S.; Kondo, M.; Sakagami, H.; Kobayashi, O.; Ishimoto, T.; Shinozaki, K. Dual Emission from an Iridium(iii) Complex/counter Anion Ion Pair. *Dalton Trans.* **2021**, *50*, 1887−1894.

(8) Zamora, A.; Vigueras, G.; Rodríguez, V.; Santana, M. D.; Ruiz, J. Cyclometalated Iridium(III) Luminescent Complexes in Therapy and Phototherapy. *Coord. Chem. Rev.* **2018**, *360*, 34−76.

(9) Li, X.; Wu, J.; Wang, L.; He, C.; Chen, L.; Jiao, Y.; Duan, C. Mitochondrial-DNA-Targeted Ir III -Containing Metallohelices with Tunable Photodynamic Therapy Efficacy in Cancer Cells. *Angew. Chem., Int. Ed.* **2020**, *59*, 6420−6427.

(10) Iqbal, N.; Jung, J.; Park, S.; Cho, E. J. Controlled Trifluoromethylation Reactions of Alkynes through Visible-Light Photoredox Catalysis. *Angew. Chem., Int. Ed.* **2014**, *53*, 539−542.

(11) Choi, S.; Chatterjee, T.; Choi, W. J.; You, Y.; Cho, E. J. Synthesis of Carbazoles by a Merged Visible Light Photoredox and Palladium-Catalyzed Process. *ACS Catal.* **2015**, *5*, 4796−4802.

(12) Chatterjee, T.; Iqbal, N.; You, Y.; Cho, E. J. Controlled Fluoroalkylation Reactions by Visible-Light Photoredox Catalysis. *Acc. Chem. Res.* **2016**, *49*, 2284−2294.

(13) Prier, C. K.; Rankic, D. A.; MacMillan, D. W. C. Visible Light Photoredox Catalysis with Transition Metal Complexes: Applications in Organic Synthesis. *Chem. Rev.* **2013**, *113*, 5322−5363.

(14) Shaw, M. H.; Twilton, J.; MacMillan, D. W. C. Photoredox Catalysis in Organic Chemistry. *J. Org. Chem.* **2016**, *81*, 6898−6926.

(15) Marzo, L.; Pagire, S. K.; Reiser, O.; Kçnig, B. Visible-Light Photocatalysis: Does It Make a Difference in Organic Synthesis? *Angew. Chem., Int. Ed.* **2018**, *57*, 10034−10072.

(16) Romero, N. A.; Nicewicz, D. A. Organic Photoredox Catalysis. *Chem. Rev.* **2016**, *116*, 10075−10166.

(17) Allen, L. J.; Cabrera, P. J.; Lee, M.; Sanford, M. S. N-Acyloxyphthalimides as Nitrogen Radical Precursors in the Visible Light Photocatalyzed Room Temperature C−H Amination of Arenes and Heteroarenes. *J. Am. Chem. Soc.* **2014**, *136*, 5607−5610.

(18) Nakafuku, K. M.; Fosu, S. C.; Nagib, D. A. Catalytic Alkene Difunctionalization via Imidate Radicals. *J. Am. Chem. Soc.* **2018**, *140*, 11202−11205.

(19) Cambié, D.; Bottecchia, C.; Straathof, N. J. W.; Hessel, V.; Noël, T. Applications of Continuous-Flow Photochemistry in Organic Synthesis, Material Science, and Water Treatment. *Chem. Rev.* **2016**, *116*, 10276−10341.

(20) Soni, V. K.; Hwang, H. S.; Moon, Y. K.; Park, S. W.; You, Y.; Cho, E. J. Generation of N-Centered Radicals via a Photocatalytic Energy Transfer: Remote Double Functionalization of Arenes Facilitated by Singlet Oxygen. *J. Am. Chem. Soc.* **2019**, *141*, 10538−10545.

(21) Liu, W. Q.; Lei, T.; Song, Z. Q.; Yang, X. L.; Wu, C. J.; Jiang, X.; Chen, B.; Tung, C. H.; Wu, L. Z. Visible Light Promoted Synthesis of Indoles by Single Photosensitizer under Aerobic Conditions. *Org. Lett.* **2017**, *19*, 3251−3254.

(22) Tomita, R.; Yasu, Y.; Koike, T.; Akita, M. Combining Photoredox-Catalyzed Trifluoromethylation and Oxidation with DMSO: Facile Synthesis of α-Trifluoromethylated Ketones from Aromatic Alkenes. *Angew. Chem., Int. Ed.* **2014**, *53*, 7144−7148.

(23) Yoshihara, T.; Yamaguchi, Y.; Hosaka, M.; Takeuchi, T.; Tobita, S. Ratiometric Molecular Sensor for Monitoring Oxygen Levels in Living Cells. *Angew. Chem., Int. Ed.* **2012**, *51*, 4148−4151.

(24) Kando, A.; Hisamatsu, Y.; Ohwada, H.; Itoh, T.; Moromizato, S.; Kohno, M.; Aoki, S. Photochemical Properties of Red-Emitting Tris(cyclometalated)Iridium(III) Complexes Having Basic and Nitro Groups and Application to pH Sensing and Photoinduced Cell Death. *Inorg. Chem.* **2015**, *54*, 5342−5357.

(25) Turro, N. J.; Ramamurthy, V.; Scaiano, J. C. *Modern Molecular Photochemistry of Organic Molecules*; University Science Books: Sausalito, CA, 2010.

(26) Martinez, L. J.; Scaiano, J. C. Characterization of the Transient Intermediates Generated from the Photoexcitation of Nabumetone: A Comparison with Naproxen. *Photochem. Photobiol.* **1998**, *68*, 646−651.

(27) Kawamura, Y.; Brooks, J.; Brown, J. J.; Sasabe, H.; Adachi, C. Intermolecular Interaction and a Concentration-Quenching Mechanism of Phosphorescent Ir(III) Complexes in a Solid Film. *Phys. Rev. Lett.* **2006**, *96*, 017404.

(28) Reineke, S.; Schwartz, G.; Walzer, K.; Falke, M.; Leo, K. Highly Phosphorescent Organic Mixed Films: The Effect of Aggregation on Triplet−Triplet Annihilation. *Appl. Phys. Lett.* **2009**, *94*, 163305.

(29) Song, D.; Zhao, S.; Luo, Y.; Aziz, H. Causes of Efficiency Roll-Off in Phosphorescent Organic Light Emitting Devices: Triplet−Triplet Annihilation versus Triplet−Polaron Quenching. *Appl. Phys. Lett.* **2010**, *97*, 243304.

(30) Namdas, E. B.; Ruseckas, A.; Samuel, I. D. W.; Lo, S.-C.; Burn, P. L. Photophysics of fac-Tris(2-Phenylpyridine) Iridium(III) Cored Electroluminescent Dendrimers in Solution and Films. *J. Phys. Chem. B* **2004**, *108*, 1570−1577.

(31) D ' Andrade, B.; Forrest, S. R. Formation of Triplet Excimers and Dimers in Amorphous Organic Thin Films and Light Emitting Devices. *Chem. Phys.* **2003**, *286*, 321−335.

(32) Bleiholder, C.; Gleiter, R.; Werz, D. B.; Köppel, H. Theoretical Investigations on Heteronuclear Chalcogen−Chalcogen Interactions: On the Nature of Weak Bonds between Chalcogen Centers. *Inorg. Chem.* **2007**, *46*, 2249−2260.

(33) Khanh, P. N.; Phan, C. D.; Ho, D. Q.; Vo, Q. V.; Ngan, V. T.; Nguyen, M. T.; Trung, N. T. Insights into the Cooperativity between Multiple Interactions of Dimethyl Sulfoxide with Carbon Dioxide and Water. *J. Comput. Chem.* **2019**, *40*, 464−474.

(34) Lutkus, L. V.; Rickenbach, S. S.; McCormick, T. M. Singlet Oxygen Quantum Yields Determined by Oxygen Consumption. *J. Photochem. Photobiol., A* **2019**, *378*, 131−135.